AD-A199 396

IMENTATION PAGE

Form Approved
OMB No 0704-0188
Exp Date Jun 30 1986

1a REPORT SECURITY CLASSIFICATION UNCLASSIFIED	1b RESTRICTIVE MARKINGS
2a SECURITY CLASSIFICATION AUTHORITY	3 DISTRIBUTION/AVAILABILITY OF REPORT Approved for public release; distribuiton unlimited
2b DECLASSIFICATION/DOWNGRADING SCHEDULE	
4 PERFORMING ORGANIZATION REPORT NUMBER(S) USAMRICD-P86-014	5 MONITORING ORGANIZATION REPORT NUMBER(S) USAMRICD-P86-014
6a NAME OF PERFORMING ORGANIZATION US Army Medical Research Institute of Chemical Defense 6b OFFICE SYMBOL (If applicable) SGRD-UV-YN	7a NAME OF MONITORING ORGANIZATION US Army Medical Research Institute of Chemical Defense, SGRD-UV-RC
6c ADDRESS (City, State, and ZIP Code) Aberdeen Proving Ground, MD 21010-5425	7b ADDRESS (City, State, and ZIP Code) Aberdeen Proving Ground, MD 21010-5425
8a NAME OF FUNDING/SPONSORING ORGANIZATION 8b OFFICE SYMBOL (If applicable)	9 PROCUREMENT INSTRUMENT IDENTIFICATION NUMBER
8c ADDRESS (City, State, and ZIP Code)	10 SOURCE OF FUNDING NUMBERS PROGRAM ELEMENT NO. / PROJECT NO / TASK NO. / WORK UNIT ACCESSION NO.

11 TITLE (Include Security Classification)
The Inferior Olivary Complex of Guinea Pig: Cytoarchitecture and Cellular Morphology

12 PERSONAL AUTHOR(S)
Foster, RE and Peterson, BE

13a TYPE OF REPORT	13b TIME COVERED	14 DATE OF REPORT (Year, Month, Day)	15 PAGE COUNT
Open Lit	FROM _____ TO _____	1986	16

16 SUPPLEMENTARY NOTATION
Publ is Brain Research Bulletin, Vol 17, pp 785-800, 1986

17 COSATI CODES			18 SUBJECT TERMS (Continue on reverse if necessary and identify by block number)
FIELD	GROUP	SUB-GROUP	Guinea Pig, Inferior olive, Golgi stain, Stereotaxic atlas; HRP injection, Dendrites, Morphometry, Neuronal form

19 ABSTRACT (Continue on reverse if necessary and identify by block number)

The inferior olivary complex (IOC) of the guinea pig can be divided into three primary subdivisions: the principal olive (PO), the medial accessory olive (MAO), and the dorsal accessory olive (DAO). In Nissl-stained preparations, the PO possessed darker staining cells than did the MAO and DAO and was the most densely populated with cells. All neuronal somata in the OOC were oblique-spheroid in profile (mean size: coronal=18.3 um, para-sagittal=15.8 um). Based on Golgi impregnations, it was apparent that inferior olive cells were of two unique radiate-cell types (I and II). Type I neurons had relatively diffuse, sparsely branched dendritic arbors, whereas type II cells and dendrites which were highly branched and massed about the cell body, at times creating complex spirals. Type II cells were further categorized into types IIa and IIb based on geometric variations of the type II dendritic arbors. Indices of branching and tortuosity, together with estimates of dendritic arbor volume, were quite helpful in distinguishing cell types. The cell types were differentially distriubted across the subdivisions with type I neurons being

20 DISTRIBUTION/AVAILABILITY OF ABSTRACT	21 ABSTRACT SECURITY CLASSIFICATION
☐ UNCLASSIFIED/UNLIMITED ☒ SAME AS RPT ☐ DTIC USERS	UNCLASSIFIED
22a NAME OF RESPONSIBLE INDIVIDUAL Jaax, nancy K, LTC, VC	22b TELEPHONE (Include Area Code) (301) 671-2553 / 22c OFFICE SYMBOL SGRD-UV-Y

DD FORM 1473, 84 MAR — 83 APR edition may be used until exhausted. All other editions are obsolete.

SECURITY CLASSIFICATION OF THIS PAGE

UNCLASSIFIED

19. Abstract (cont'd)

encountered in the MAO while type II cells were found in all three subdivisions. Within the neuropil of the IOC, three different afferent axonal arbors were identified, as was the presence of dendrites from surrounding reticular formations cells. Neuronal aggregates creating a possible electrical syncytium within the IOC are consistent with the dendroarchitectonics of the cells.

Brain Research Bulletin, Vol. 17, pp. 785–800, 1986. Ankho International Inc. Printed in the U.S.A. 0361-9230/86 $3.00 + .00

The Inferior Olivary Complex of Guinea Pig: Cytoarchitecture and Cellular Morphology[1]

ROBERT E. FOSTER[2] AND BETH E. PETERSON

Comparative Pathology Branch, Pathophysiology Division
U.S. Army Medical Research Institute of Chemical Defense, Aberdeen Proving Ground, MD 21010-5425

Received 12 June 1986

FOSTER, R. E. AND B. E. PETERSON. *The inferior olivary complex of guinea pig: Cytoarchitecture and cellular morphology.* BRAIN RES BULL 17(6) 785–800, 1986.—The inferior olivary complex (I.O.C.) of the guinea pig can be divided into three primary subdivisions: the principal olive (PO), the medial accessory olive (MAO), and the dorsal accessory olive (DAO). In Nissl-stained preparations, the PO possessed darker staining cells than did the MAO and DAO and was the most densely populated with cells. All neuronal somata in the I.O.C. were oblique-spheroid in profile (mean size: coronal = 18.3 μm, parasagittal = 15.8 μm). Based on Golgi impregnations, it was apparent that inferior olive cells were of two unique radiate-cell types (I and II). Type I neurons had relatively diffuse, sparsely branched dendritic arbors, whereas type II cells had dendrites which were highly branched and massed about the cell body, at times creating complex spirals. Type II cells were further categorized into types IIa and IIb based on geometric variations of the type II dendritic arbors. Indices of branching and tortuosity, together with estimates of dendritic arbor volume, were quite helpful in distinguishing cell types. The cell types were differentially distributed across the subdivisions with type I neurons being encountered in the MAO while type II cells were found in all three subdivisions. Within the neuropil of the I.O.C., three different afferent axonal arbors were identified, as was the presence of dendrites from surrounding reticular formation cells. Neuronal aggregates creating a possible electrical syncytium within the I.O.C. are consistent with the dendroarchitectonics of the cells.

Guinea pig Inferior olive Golgi stain Stereotaxic atlas HRP injection Cytoarchitecture
Dendrites Morphometry Neuronal form Typologic conservatism

RECENT intracellular electrophysiological studies of guinea pig inferior olive (I.O.) neurons have revealed the distinct and characteristic cellular property of an oscillating membrane potential [4, 23, 27]. The oscillatory phenomenon appeared in a sampling of neurons from all of the subdivisions of the inferior olivary complex (I.O.C.) [4], and it was shown that the oscillations could be altered by afferents coursing into the I.O.C. from its dorsal aspect [4]. In addition, morphological information derived from injections of the fluorescent dye Lucifer yellow revealed that aggregates of inferior olive neurons are dye-coupled, presumably through gap junctions between dendrites, and that at least two distinct cell types exhibited the oscillatory behavior [4].

While the inferior olivary complex in several species of mammal has been the object of anatomical analyses (e.g., [6, 7, 17, 19, 20, 35, 41, 42]), little is known about the inferior olive of the guinea pig. Our Lucifer yellow labeling of I.O. neurons in brain slices maintained *in vitro* suggested that the diversity of I.O. cell types described by Ramón y Cajal [35] and the Scheibels [41] for several mammals were represented in the guinea pig. The data demonstrating Lucifer yellow dye-coupling [47] between I.O. cells might have been predicted based on the demonstrations of gap junctions in the I.O.C. [4, 17, 19, 40, 46]. In addition, a neuronal aggregate organization of the type illustrated in the Scheibel's Golgi analyses (Figs. 14 and 15 in [41]) was supported by the labeling of multiple cells from the Lucifer yellow injection into only one I.O. neuron [4]. The early Golgi analyses also revealed at least two types of afferent axonal arbors in the I.O.C. of mouse, cat and monkey [35, 41, 42]. Therefore, with the electrophysiological studies and previous Golgi analyses in mind, a conventional neuroanatomical study of the cytoarchitecture and cellular morphology of the guinea pig inferior olive was undertaken as an antecedent to further electrophysiological studies. This report presents data relevant to several questions concerning the guinea pig I.O.C.:

[1]The opinions or assertions contained herein are the private views of the authors and are not to be construed as Official or as reflecting the views of the U.S. Army or the Department of Defense. In conducting the research described in this report, the investigators adhered to the "Guide for the Care and Use of Laboratory Animals" of the Institute of Laboratory Animal Resources, National Research Council.

[2]Requests for reprints should be addressed to Commander, U.S. Army Medical Research Institute of Chemical Defense, Attn. SGRD-UV-YC/Dr. Robert Foster, Aberdeen Proving Ground, MD 21010-5425.

(1) What is the cytoarchitecture of the inferior olive in stereotaxic coordinates? (2) Based on dendritic morphology, what are the cell types of the inferior olive and what is their distribution? (3) What are the general and statistical characteristics of the dendritic trees? and (4) What axon types are represented in the inferior olive?

METHOD

Cytoarchitecture and Stereotaxic Atlas

The brains of 8 guinea pigs, *Cavia porcelus* (Hartley strain) weighing 300–400 g, were used. Prior to the stereotaxic insertion of coordinate reference pins into a brain, an animal was anesthetized with sodium pentobarbital (40 mg/kg IP) and perfused transcardially with 200 ml of Ringer's solution followed by 1000 ml of formaldehyde (1% formaldehyde in 0.1 M phosphate buffer, pH 7.3). The head was positioned in a stereotaxic instrument (Kopf 1700) such that the cranial sutures lambda and bregma were coplanar in the horizontal plane. This procedure set the incisor bar at −12.0 mm referenced to the interaural line. Following the placement of coordinate-reference pins, the brain was removed, frozen on powdered dry ice, and mounted for sectioning at 20 μm in a Slee type HS cryostat. Sections were thaw mounted on subbed glass microscope slides, air dried and stored at room temperature in slide boxes. Sections to be used for cytoarchitectonic analyses were stained for Nissl substance with cresyl violet by conventional procedures, dehydrated in ethanol, cleared in xylene, and coverslipped under Permount. Inferior olive cytoarchitectural features were traced onto drawings of serial sections (100 μm intervals at least) and referenced to stereotaxic coordinates by plotting the position of the reference pin artifacts on the drawings.

Measurement of soma dimensions (see the Data Analyses section below) in the three major subdivisions of the inferior olive utilized 2 brains which were not fixed prior to freezing. The fresh brains were removed from the calvarium following deep anesthesia and decapitation with guillotine. The brains were glued to a cryostat chunk and frozen in powdered dry ice. Sectioning, slide mounting and Nissl staining procedures were as outlined above.

Golgi Stain, HRP Injection

Fifteen brains, stained by a modification [1] of the del Rio-Hortega Golgi procedure for aldehyde-fixed tissue, were examined to assess the dendritic morphology of inferior olive neurons. After the staining period (3 days in mordant, 3 days in silver nitrate), 150–250 μm sections were taken from the 3 mm thick tissue slabs either by tissue chopping or by vibratome. The sections were collected in fresh phosphate buffer, dehydrated in ethanols, cleared in α-terpineol, rinsed in xylene, mounted, and coverslipped. Cytoarchitectonic analysis of the position of impregnated cells was performed on selected sections after the cells had been analyzed for their three-dimensional tree structure properties. These sections were removed from the glass slide in a xylene bath, rehydrated through ethanols to water and processed for cresyl violet counterstaining according to the procedure of Geisert and Updyke [14]. The cresyl violet staining was carried out at 37°C for 30 minutes followed by conventional dehydration and differentiation in ethanol-acetic acid.

Rapid Golgi preparations from 10, 10–12 day prepartal guinea pigs were examined for axonal staining in the inferior olive. The mother was anesthetized with sodium pentobarbital (40 mg/kg, IP) and the fetuses were removed. The fetal brains were removed and cut into 3 mm thick slabs, and subsequently placed in the rapid Golgi mordant [32]. Further processing of the brains was according to the procedures of Morest [32].

Iontophoretic injections of horseradish peroxidase (HRP; Sigma Type IV) into I.O. neurons were carried out in tissue slices maintained *in vitro* [4] in order to correlate dendritic morphology with electrophysiological characteristics of inferior olive cells. HRP (10% in Tris buffer, pH 7.6) was injected intracellularly via glass capillary micropipettes (W-P Instruments, TWF-120). Injections were made in only those I.O. neurons that demonstrated the characteristic oscillatory behavior and that had an initial resting membrane potential of −45 mV or lower. Successful injections were made by applying hyperpolarizing pulses (500 msec duration, 1 Hz) to the micropipette for at least 2 min. After the injection the tissue slice was kept in the chamber at least 30 minutes prior to its removal and fixation in 1% neutral-buffered formaldehyde. Conventional HRP histochemistry was carried out using DAB (diaminobenzidene tetrahydrochloride) as the chromagen. The brain slices with injected neurons were then dehydrated in ethanol, cleared in xylene, mounted on glass microscope slides and coverslipped under Permount.

Data Analyses

Standard two-dimensional analyses of dendritic and axonal architecture of I.O. neurons were carried out by microscopic examination and camera lucida drawings. Zeiss oil immersion optics were used exclusively. Only those neurons with the characteristics of complete impregnation, little overlap with other stained cells, and few sectioned dendrites were chosen for further analyses. In these cases, each dendrite was drawn separately under camera lucida and a composite drawing of all dendrites was constructed. Using the composite drawing as an orientation map, the linear dimensions of the cell's dendritic tree were then digitized into a Cartesian coordinate database [16, 51, 55–58] with a centrifugal ordering of dendritic segments [15,49]. The digitization was carried out with a Zeiss Universal microscope (100x Neofluor, NA 1.0, oil immersion objective; 0.5 μm X-Y stepping stage, 0.1 μm stepping Z-axis) driven by a Zeiss Zonax controller which was slaved to host minicomputer.

Dendritic tree structure analyses were carried out using the database representation of the complete three-dimensional dendritic arbors. These analyses included the following: (1) stick-figure representation of the dendritic tree in any plane of section (Fig. 4), (2) Sholl diagrams [44], (3) trumpet and polar histogram analyses [16], (4) principal component analysis [57], (5) the topological descriptor called branching index (B.I. = No. of dendritic end points ÷ No. of 1st order dendrites; increasing B.I. values indicated that more dendrites of the cell had higher branch orders), (6) geometrical parameters such as indices of flatness (I.F.) and axialization (I.A.) [57] and an index of tortuosity (I.T. = total length of dendritic segments from the origin point on the cell body to the end point ÷ length of a vector from dendrite origin point on the soma to dendrite end; I.T. = 1 would be a straight line; a larger I.T. indicates that a longer dendrite turns back and ends closer to its somatic origin point), and (7) metrical parameters such as length of the longest dendrite, total dendritic length, mean dendritic length, and mean length of a dendritic segment.

In addition, for each Golgi-impregnated cell analyzed in detail, volume and surface area statistics were estimated for the dendritic arbor alone and for the total cell (dendritic arbor + cell body). In order to calculate these estimates, three pieces of data were used: (1) the length of each segment of each dendrite, (2) the diameter of each dendritic segment, and (3) the equivalent diameter of the cell body. The dendritic segment lengths were derived from the digitized database of a cell's dendritic arbor. The estimated diameter of each dendritic segment was taken as the average of segment widths measured at several intervals along the camera lucida drawing of each segment. The average width of a segment was then cross-checked by measurement with an ocular micrometer through high magnification microscopic examination of the cell. It should be noted that, except for the initial portions of the 1st order dendrite, dendritic taper was negligible or beyond our analytical techniques. For this reason, all of the volume and area calculations reported have assumed that dendritic segments were cylinders. Finally, the diameter of the cell body was estimated by the E.C.D. procedure (see below) utilizing the outline of the soma from the camera lucida drawing of the cell. The soma was then assumed to be spherical and the area and volume calculated.

Analysis of distribution of soma dimensions across the I.O. subdivisions was carried out by utilizing two estimation procedures for equivalent soma diameter. The major subdivisions of the inferior olive were identified in Nissl-stained, 20 μm fresh frozen sections, and the outlines of 30 cells from each subdivision and two planes of cut (i.e., 60 cells per subdivision; 180 cells total) were drawn at 1000× with camera lucida. The two criteria for cell selection were the presence of a nucleus and a nucleolus. The diameter of each selected cell was then estimated by two techniques. For the first, outlines of each cell were digitized with a computer assisted planimeter and the area was calculated. From the cell body area, an equivalent circle diameter (E.C.D.) was derived for each cell. For the second, the estimate of soma diameter was derived by averaging the lengths of two orthogonal lines which describe the subjective minimum and maximum axes of the cell's cross sectional profile (Min-Max D.). From each technique, standard mean statistics were calculated for a total of eight sets of I.O. cells (i.e., all I.O. cells in coronal plane; all I.O. cells in parasagittal plane; and, 6 additional sets = 3 subdivisions × 2 planes of cut). The population statistics for each set were then compared by standard statistical tests for mean differences. It is interesting to note that both estimation procedures yielded similar descriptive statistics, although the Min-Max D. technique had more population variance, the result of which was inconsistency in the 'between population' comparisons of mean differences (Table 2). Because of this observation we chose the E.C.D. procedure for cell diameter estimation in the Golgi analyses.

Our presentation of the anatomical characteristics of each type of I.O. neuron will reference Tables 2–4 which contain many numeric parameters of the six cells that were chosen as representative of the cell types in the guinea pig I.O.C. These parameters are presented for three purposes: (1) to illustrate those measurements or indices that were or were not useful in cell categorization within the I.O.C., (2) to provide an initial database of cellular morphometry for anatomical comparisons within the guinea pig brain and across species, and (3) to provide a catalog of those cellular statistics, which can be used to construct anatomical and/or physiological models [34] of these interesting cells.

RESULTS

Stereotaxic Coordinates and Cytoarchitecture of the Inferior Olivary Complex

The I.O.C. in the guinea pig extends for approximately 3 mm along the ventral surface of the medulla oblongata from the level of the obex rostral to the level of the caudal pole of the VIIth cranial nerve nucleus. The I.O.C. is bounded ventromedially by the pyramidal tract and laterally, for 1.5 mm of its caudal extent, by the lateral reticular nucleus. The neuropil of the brainstem reticular formation forms the dorsal boundary of the I.O.C. The extent of the I.O.C. in Kopf-stereotaxic coordinates and a parcellation of the I.O.C. into the subdivisions proposed for the rat [17] are illustrated in Fig. 1.

As in other rodents [6,17], the I.O.C. of the guinea pig could be separated into three primary subdivisions based on the cytoarchitectonic criteria of cell packing density (Table 1), intensity of Nissl-stain, and the topology of cell groupings. Cell size (Table 1 and see below) was not a useful criterion for the cytoarchitectonic parcellation. The medial accessory olive (MAO; solid in Fig. 1) begins as the most caudal subdivision and extends through the complete caudal-rostral axis of the I.O.C. The MAO can be further subdivided into five topological subgroups [6] (Fig. 1; a, b, c, β, dc). The dorsal accessory olive (DAO; stippled in Fig. 1) and principal olive (PO and vl; clear in Fig. 1) begin at least 1 mm rostral to the caudal pole of the I.O.C. The PO occupies an intermediate position between the MAO and DAO and extends to within 0.5 mm of the rostral pole of the I.O.C. The DAO, positioned lateral to the MAO and PO, extends to the extreme rostral pole of the I.O.C.

A unique feature of the I.O.C. in the guinea pig is the existence of a compact group of large isodendritic neurons, the *periolivary reticular nucleus* (R, Fig. 1 top and bottom), which is positioned ventral to the DAO and PO (A-P −3.28; Fig. 1). This cell group extends for approximately 0.5 mm near the middle of the rostral-caudal axis of the I.O.C. These isodendritic [38] cells have the cytological characteristics of neurons in lateral reticular nucleus and, in fact, the cells may represent a ventromedial extension of that nucleus. While large isodendritic cells have been seen in the I.O.C. of other mammals [7, 35, 41], the collection of these cells into a discrete group has not been previously described. In addition to the large neurons of the compact periolivary reticular nucleus, scattered large isodendritic neurons were evident at the ventral margins of the subdivisions, sometimes interposed in the hilar space between the DAO and PO (Fig. 6 bottom). These cells were similar in their cytological characteristics of staining and size to the cells in the periolivary reticular nucleus.

Morphological Characteristics of the I.O. Neuronal Somata

The cytological characteristics of the somata of Nissl-stained neurons in the three subdivisions were similar in terms of the distribution of Nissl substance. However, the cells of the PO were more darkly stained and more densely packed (Table 1) than those of the MAO and DAO, characteristics which were often used to delineate the cytoarchitectonic boundaries between the subdivisions at areas of confluence. Unlike the I.O.C. in other mammals [35,41], no laminar alignment of cell bodies was apparent in the subdivisions of the guinea pig I.O. Throughout the I.O.C. the cells were ovoid to round in shape with relatively uniform

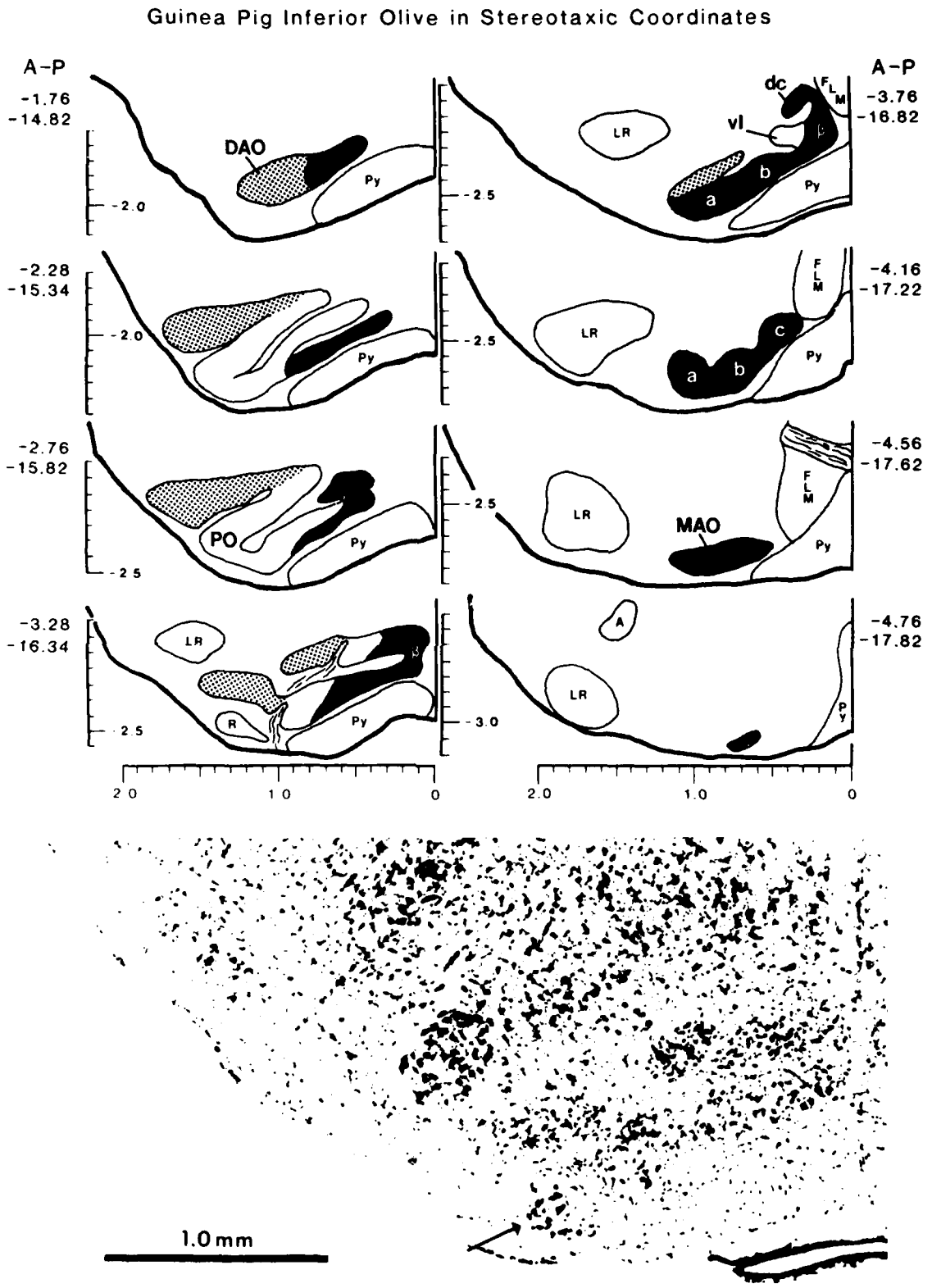
Guinea Pig Inferior Olive in Stereotaxic Coordinates
A-P
-1.76
-14.82
DAO
Py
-2.0
-2.28
-15.34
-2.76
-15.82
PO
-2.5
-3.28
-16.34
LR
R
A-P
-3.76
-16.82
dc
vl
a
b
-2.5
-4.16
-17.22
c
-4.56
-17.62
MAO
-4.76
-17.82
A
-3.0
2.0
1.0
0
1.0 mm

FIG. 1.

TABLE 1

CELL SIZE, CELL PACKING DENSITY, AND DISTRIBUTION OF CELL TYPES IN THE INFERIOR OLIVE

I.O. Subdivision	Mean Soma Diameter E.C.D. from Area (microns ± S.D., n=30) Coronal	Parasagittal	Mean Soma Diameter Min-Max D. (microns ± S.D., n=30) Coronal	Parasagittal	Packing Density (cells × 1000/mm³)	Cell Type Distribution Ia	IIa	IIb
MAO	17.8 ± 1.6	14.9 ± 1.8†	16.9 ± 1.6	15.3 ± 2.2*	16.8–30.5	+++	NE	+
range	(14.8–20.8)	(11.8–18.2)	(14.6–19.3)	(12.2–18.4)				
DAO	18.4 ± 1.6	16.0 ± 2.1†	18.1 ± 1.5	14.8 ± 1.8†	16.0–20.2	NE	++	+
range	(15.2–21.4)	(12.2–21.6)	(14.6–21.5)	(11.7–17.9)				
PO	18.6 ± 1.6	16.4 ± 1.8†	17.7 ± 1.6	16.4 ± 1.9	28.2–54.9	NE	+++	++
range	(15.4–21.2)	(13.8–20.0)	(14.5–20.9)	(12.3–20.5)				

Key: E.C.D.: equivalent circle diameter calculated from cell area measurement.
Min-Max D.: mean minimum-maximum diameter (min + max ÷ 2).
NE: None encountered.
+: Relative density (+++ = most dense).
S.D.: standard deviation
Bonferroni significance levels: *significantly different from coronal plane at $p=0.05$, pairwise t-test; †significantly different from coronal plane at $p=0.001$, pairwise t-test.

distribution of Nissl substance in the cytoplasm and a large, centrally located nucleus. Typically, the nucleus contained a single nucleolus which exhibited normal dense staining characteristics.

Visual examination under low magnification showed neither size nor shape differences among the neurons within the three subdivisions of the I.O.C. In order to quantify this visual impression, a sampling of neurons from each subdivision was analyzed for an estimate of equivalent soma diameter using two procedures. The results of these procedures are presented in Table 1. Interestingly, neurons from all three subdivisions cut in the parasagittal plane have a significantly smaller profile (mean=15.8 μm; range=11.8–21.6 μm) than those cut in the coronal plane (mean=18.3 μm; range=14.8–21.4 μm). This suggests an oblique spheroid-shaped cell body with the long axis oriented in the coronal plane.

In Golgi preparations, the oblong shape of the impregnated cell bodies confirmed the description from Nissl-stained cells. The somata of some neurons exhibited thorny protuberances (Fig. 2, cell B), whereas other cells had relatively smooth cell bodies (e.g., Fig. 4). The existence of somatic appendages did not seem to be correlated with cell type or location. Finally, the somata of all I.O. neurons gave rise to an axon hillock and at least 7 dendritic trunks.

Morphological Characteristics of the Dendrites

An initial examination of the dendrites from the Lucifer yellow-filled cells illustrated in the preceding report [4], suggested that I.O. neurons displayed two basic types of dendritic morphology, an unbranched *simple* idiodendritic [37,38] type (type I) and a highly branched, sometimes tightly-wound *complex* idiodendritic type (type II). Our analyses of Golgi-impregnated and HRP-filled I.O. neurons confirmed the presence of the two basic types, but indicated that the type II classification needed further division into type IIa and IIb categories; the type IIb (Fig. 2, cell C) cell being a transitional form between the relatively unbranched type I (Fig. 2, cell B) and the tightly wound type IIa (Fig. 2, cell E).

Visual classification of I.O. neurons based on dendritic geometry led us to question whether a statistical description of the dendritic arbor could be utilized for a more objective classification of the cells. Six cells, spanning our subjective classification of the three cell types, were chosen for the analysis and their dendritic trees were digitized for three-dimensional reconstruction using a computer-assisted microscope. From the three-dimensional database for each cell, stick figures of each were generated in the section plane and the two other standard planes of cut (Fig. 5). In addition, several statistics were derived from the da-

FACING PAGE

FIG. 1. TOP—Stereotaxic atlas of the inferior olive in guinea pig in the coronal plane. All coordinates (in mm) are for a Kopf 1700 series stereotaxic instrument with the guinea pig adapter incisor bar set at −12.0 mm. The anterior-posterior (A-P) coordinates are referenced to the interaural line (top value) and to the bregma skull suture (bottom value). The vertical coordinates (left of each section) are referenced to the interaural line (0.0 mm). The three primary subdivisions of the I.O. are indicated as follows: the medial accessory olive (MAO) and its subdivisions (a, b, c, β, dc) are in black; the dorsal accessory olive (DAO) is stippled; the principal olive (PO) and the ventrolateral extension of the dorsal cell column (vl) are not shaded. The unique periolivary reticular nucleus (R) is located just lateral to the emergence of the hypoglossal nerve. Other structures illustrated include the pyramidal tract (Py), medial longitudinal fasciculus (FLM), nucleus ambiguus (A), and the lateral reticular nucleus (LR). BOTTOM—Low power photomicrograph of a Nissl-stained section through the inferior olive at the level of the 'periolivary reticular nucleus.' This section is from the A-P coordinate of −3.28 mm (see Fig. 1, top). The arrow points to assembly of large neurons called the periolivary reticular nucleus.

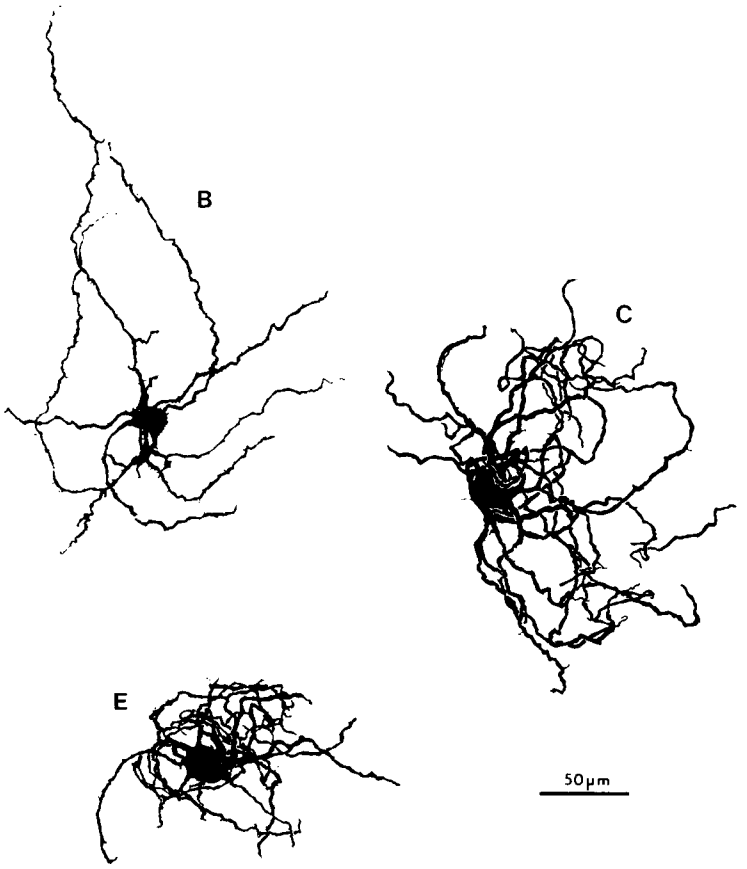

FIG. 2. Camera lucida drawings of Golgi-impregnated inferior olive neurons illustrating the three cell types. The three cells are labeled (B,C,E) according to their position in Fig. 5. The type I neuron at upper left is clearly different from the type IIa cell at lower left and the type IIb cell at center right. The type IIb neuron is considered as transitional between types I and IIa based on statistical description of its dendritic arbor.

tabase, including (1) dendritic length, area, and volume, (2) indices of the axialization, flatness, branching, and tortuosity of the dendritic tree, and (3) a measure of volume (V.D.E.; volume of the dendritic extent) which defines the smallest box that just circumscribes the dendritic tree (calculated from the outside dimensions of the three 'principal planes' [57] of the cell). The stick figures of each cell in the three cardinal section planes are shown in Fig. 5, and the statistics on the six representative cells are summarized in Tables 2, 3 and 4. The stick figures of Fig. 5 are organized such that type I neurons are represented by cells A and B, type IIb transitional neurons by cells C and D, and type IIa neurons by cells E and F. The statistics for these cells (Tables 2–4) show that dendritic length, area and volume (Table 3) as well as indices of axialization (I.A.; Table 2) and flatness (I.F.; Table 2) are much the same for all six cells (based on the values of I.A. and I.F., all the dendritic arbors can be described as ellipsoid). On the other hand, the index of tortuosity (I.T.; Table 2) and the branching index (B.I.; Table 2)

TABLE 2

DESCRIPTIVE INDICES OF THE DENDRITIC ARBORS OF SIX I.O. NEURONS

		Index of Tortuosity				PCA Indices	
Cell	Cell Type	Max	Min	Mean	B.I.	I.A.	I.F.
A	I	2.6	1.2	1.8	2.3	0.3	0.6
B	I	1.9	1.3	1.6	1.9	0.4	0.6
C	IIb	3.7	1.6	2.4	2.9	0.2	0.5
D	IIb	6.9	1.4	3.2	3.1	0.5	0.8
E	IIa	4.9	1.7	2.8	3.9	0.2	0.5
F	IIa	24.8	1.3	7.5	3.4	0.2	0.3

B.I. = branching index (No. dendrite tips ÷ No. dendrites).
PCA = principal component analysis.
I.A. = index of axialization.
I.F. = index of flatness.

TABLE 3

SUMMARY STATISTICS FOR THE SIX I.O. NEURONS OF FIG. 5

Cell	Type	N.D.	S.D. (μm)	Mean D.L. (μm)	L.D. (μm)	T.D.L. (μm)	V.D.E. (mm^3)	D.S.A. (μm^2)	D.V. (μm^3)	T.C.S.A. (μm^2)	T.C.V. (μm^3)
A	I	7	16.1	218	374	3213	0.250	15,053	7332	15,867	9,516
B	I	8	17.6	154	334	2106	0.014	11,241	5049	12,214	7,902
C	IIb	8	18.1	221	343	4209	0.013	18,165	6901	19,199	10,004
D	IIb	8	20.2	204	285	3956	0.007	18,415	7748	19,696	22,562
E	IIa	8	19.7	136	212	3049	0.004	10,978	3726	13,196	7,727
F	IIa	8	19.4	265	526	5706	0.003	19,882	6473	21,063	10,294

N.D. = number of dendrites.
S.D. = soma diameter (equivalent circle).
Mean D.L. = mean dendritic length.
L.D. = length of longest dendrite.
T.D.L. = total dendritic length.
V.D.E. = volume of the dendritic extent (volume of a box into which the dendritic arbor just fits, calculated from the principal planes).
D.S.A. = total dendritic surface area.
D.V. = total dendritic volume.
T.C.S.A. = total cell surface area (D.S.A. + soma area).
T.C.V. = total cell volume (D.V. + soma volume).

together with the V.D.E. measure (Table 3) provide some discrimination between neurons such that the cell types begin to emerge. Thus, it is evident that these latter statistics provide numeric descriptors for the differing dendritic arbor geometries that were visually classified under microscopic examination.

Characteristics of Type I Neurons

As represented by the neurons illustrated in Figs. 2 (cell B), 5A and B, the dendrites of type I cells characteristically leave the cell and spread diffusely with a minimum of hooking and turning back toward the soma. This lack of dendritic tortuosity is confirmed by a low mean index of tortuosity (I.T.) of approximately 1.8 (Table 3) for cells A and B and the restricted range of the I.T. for each dendrite (Table 4). The dendrites also did not exhibit branching beyond the third order, and third order branches were rare, as indicated by a B.I. around 2.0. Interestingly, several dendrites of cells A and B extended beyond 100 μm from the cell body without branching, while others branch within 25 μm of the cell body. The unbranched dendrites contained spines and other appendages, and so the possibility of their being axons was ruled out. This feature of *several* relatively long, unbranched dendrites was a clear characteristic of the type I neuron. In addition to a low I.T. and B.I., the dendritic field of this neuron type occupies a greater dimensional space (V.D.E., Table 2) than do the type II cells. Spines were evident on both the primary and secondary dendritic branches of this neuron type, as were occasional 'moniliform threads' [41]. The latter are long thin spinous appendages that, in electron micrographs, are packed with microtubules (Foster, unpublished observations).

Characteristics of Type II Neurons

Successful Golgi-impregnations frequently exhibited seemingly impenetrable, dense tangles of impregnated cells with the uniquely elaborate dendritic ramifications of a type IIa inferior olive cell. As illustrated by the cells in Figs. 2 (cell E), 4, 5E and F, the multibranching dendrites of type IIa cells tend to mass about the soma creating a tumbleweed appearance. The maximum tortuosity indices of greater than 4.0 (Table 2) for these cells indicate the compactness and complexity of the dendritic domain. A tendency of dendrites to form extensively curling patterns and twisting spirals is illustrated by the cell in Fig. 4, which may represent the extreme of this characterisic (compare the type IIa cell in Fig. 4 to the type IIa cell of Fig. 2, cell E). A dendritic spiral (see the stereopair, Fig. 4, bottom) appeared to be of appropriate size to be encircling the soma of nearby neuron. Close examination of Fig. 4, bottom will show at least 5 spirals, suggestive of possible contacts with 5 cells (see discussion of I.O.C. neuronal aggregates). The type IIa cell typically exhibited a higher branching index than did a type I cell, in these cases a B.I. greater than 3.0 (Table 2). The compact geometry created by the combination of high branching and tortuosity indices was confirmed by a low V.D.E. measure, 0.003 and 0.004 mm^3 (V.D.E., Table 3). As with type I neurons, however, spines and other small appendages appeared to varying degrees on both the dendrites and the cell body. Also, moniliform threads were occasionally visible at the tips of complete dendrites. Finally, it appeared in each type IIa cell that at least one dendrite coursed away from the cell body without branching (Table 4).

Found in all subdivisions of the I.O., some neurons resemble in the geometric complexity of their dendritic trees a type IIa cell but also possess the broader dendritic domain characteristic of type I cells. Thus, based on the complexity of their local ramifications we classify this type of neuron in the type II category, but as a type IIb cell (Fig. 2, cell C; Fig. 3; and Fig. 5C and D). Indeed, it is apparent that the type IIb neuron represents a transition between those of type I and type IIa cells. With an intermediate branching indices, 2.9 and 3.1 in these examples, these cells exhibit branching patterns intermediate between the other types. In addition, an intermediate (2.4 and 3.2 in the examples) mean I.T. and

TABLE 4

DENDRITIC LENGTH, DIAMETER AND TORTUOSITY FOR THE NEURONS OF FIG. 5

Dendrite No.	Length (μm) of Dendrites by Branch Order 1	2	3	4	5	6	7	8	Branch Dia. (μm)	T.L. (μm)	S.A. (μm²)
Cell A											
I.T.	1.5	1.6	2.6	1.2	1.7	2.2	1.7		—	—	—
1st Order	9.2	9.5	3.9	85.2	300.0	17.3	14.6		2.8	439.8	3177.7
2nd Order	412.0	320.9	209.4	★	★	391.7	275.8		1.8	1609.7	9102.9
3rd Order	★	★	326.1	★	★	165.3	429.5		0.8	920.9	2314.6
4th Order	★	★	★	★	★	243.0	★		0.6	243.0	458.1
T.L. (μm)	421.2	330.4	539.4	85.2	300.0	817.3	719.9			3213.4*	
S.A. (μm)	2396.7	1883.4	2031.8	615.4	2168.0	3213.5	2744.5				15053.3†
Cell B											
I.T.	1.5	1.3	1.3	1.6	1.3	1.9	1.9	1.6	—	—	—
1st Order	259.2	189.8	20.5	23.8	115.3	163.3	16.5	20.0	2.2	808.4	5587.5
2nd Order	★	★	30.1	97.7	★	★	179.9	67.2	1.6	374.9	1884.5
3rd Order	★	★	305.3	★	★	★	361.3	256.3	1.3	922.9	3769.3
T.L. (μm)	259.2	189.8	355.9	121.5	115.3	163.3	557.7	343.5		2106.2*	
S.A. (μm)	1791.5	1311.8	1539.9	655.6	796.9	1128.7	2494.0	1521.2			11241.3†
Cell C											
I.T.	2.7	2.2	2.2	1.6	2.6	3.7	2.1	2.4	—	—	—
1st Order	12.9	36.1	12.4	74.9	32.5	9.4	11.2	8.0	2.7	197.2	1672.8
2nd Order	356.2	263.3	189.6	★	398.7	442.9	60.9	56.5	1.7	1768.2	9443.5
3rd Order	★	177.9	392.8	★	110.9	★	836.1	725.9	1.0	2243.7	7049.1
T.L. (μm)	369.1	477.3	594.7	74.0	542.2	452.3	908.3	790.4		4209.1*	
S.A. (μm)	2011.4	2271.0	2351.3	635.1	2753.9	2444.9	3047.4	2650.3			18165.4†
Cell D											
I.T.	3.7	3.3	2.9	1.4	1.9	2.7	6.9	2.6	—	—	—
1st Order	12.6	35.3	38.7	10.7	137.5	78.5	103.2	12.2	2.6	428.7	3501.8
2nd Order	67.1	357.6	324.6	227.6	73.5	★	283.7	41.9	1.8	1376.1	7782.0
3rd Order	764.9	★	40.9	343.1	★	★	★	355.6	1.2	1504.5	5672.2
4th Order	★	★	★	★	★	★	★	255.5	0.9	255.5	722.5
5th Order	★	★	★	★	★	★	★	63.3	0.6	63.3	119.3
6th Order	★	★	★	★	★	★	★	327.4	0.6	327.4	617.2
T.L. (μm)	844.6	392.9	404.2	581.4	211.0	78.5	386.9	1056.0		3955.6*	
S.A. (μm)	3366.2	2310.6	2305.9	2668.1	1538.8	641.2	2447.4	3136.7			18414.9†
Cell E											
I.T.	4.9	2.7	3.6	2.4	2.9	1.7	2.0	1.8	—	—	—
1st Order	12.2	4.3	35.6	22.4	19.1	17.6	8.2	133.5	2.3	252.9	1827.4
2nd Order	136.4	38.9	63.6	136.6	117.1	131.5	86.6	★	1.6	710.7	3572.5
3rd Order	140.2	158.9	387.9	110.3	231.7	132.2	149.5	★	1.0	1310.7	4117.8
4th Order	★	467.3	★	166.6	51.3	★	189.3	★	0.6	874.5	1459.9
T.L. (μm)	288.8	669.4	487.1	435.9	419.2	281.3	433.6	133.5		3048.8*	
S.A. (μm)	1214.3	1606.7	1795.6	1509.1	1551.3	1203.5	1132.6	964.7			10977.7†
Cell F											
I.T.	3.9	3.4	5.2	9.1	1.3	24.8	5.2	6.8	—	—	—
1st Order	6.4	17.8	22.1	22.1	67.6	20.9	34.0	34.5	2.6	225.4	1841.2
2nd Order	192.1	214.1	431.9	181.6	★	159.6	572.6	226.5	1.5	1978.4	9323.2
3rd Order	214.8	675.8	227.8	403.2	★	242.5	★	480.7	0.9	2244.8	6347.2
4th Order	323.6	★	★	477.3	★	456.3	★	★	0.6	1257.2	2369.8
T.L. (μm)	736.9	907.7	681.8	1084.2	67.6	879.3	606.6	741.7		5705.8*	
S.A. (μm)	2174.9	3065.2	2860.0	3076.1	552.2	2468.7	2976.1	2708.4			19881.6†

T.L. = Total length; S.A. = Surface area; I.T. = Index of tortuosity; * = Total dendritic length; † = Total dendritic surface area.

FIG. 3. Camera lucida drawing of an HRP-filled, type IIb inferior olive neuron. This cell was from a 500 μm thick brain slice cut in the horizontal plane and was labeled with HRP during an intracellular recording experiment. The membrane potential of this cell displayed the characteristic oscillatory behavior described previously. The three-dimensional reconstruction of this cell is shown in Fig. 5D.

intermediate values of the I.T. for each dendrite (Table 4) indicated a decreased tendency of these dendrites to twist, curl and swirl in comparison to the dendrites of type IIa cells. While the B.I. and I.T. of the cell in Fig. 2 (cell C) suggested that it belonged to the type II category, the V.D.E. value for the type IIb cell (Table 2, cell C) suggests that the cell is of type I variety. Thus we could have placed cells with these mixed characteristics in a separate category. However, the cells have the geometric characteristics of a type IIa cell, and for this reason, we have called them type IIb. As in the other I.O. cell types, dendritic and somatic appendages (e.g., spines, knobs, moniliform threads) were present on most type IIb cells. Finally, as in type IIa cells, at least one dendrite of the type IIb neurons exhibited no secondary branching.

Distribution of Cell Types Within the I.O.C.

Using the classification of dendrites into types I, IIa and IIb, a survey of Golgi-impregnated I.O. neurons in sections counterstained for Nissl substance was undertaken. Sections from several brains cut in the coronal plane were used and the neuron classification was carried out before counterstaining. The position of each cell encountered was indicated with a symbol for cell type on camera lucida drawings of the non-counterstained sections. Sections were then counterstained and the cytoarchitectural boundaries of the I.O. subdivisions were transcribed onto the plots of the cells by type. Table 1 summarizes the results of this survey and demonstrates that there is a parcellation of cell types into the I.O. subdivisions. Thus, the Type I neurons (e.g., Fig. 2, cell B; Fig. 5A and B) were only found in the MAO whereas the type IIa neuron (Fig. 2, cell E; Fig. 4; and Figs. 5E and F) was only encountered in PO and DAO. The transitional type IIb cell (Fig. 2, cell C; Fig. 3; Figs. 5C and D) was seen in all three subdivisions.

Other Anatomical Characteristics of the I.O.C.

I.O. dendritic fields obey cytoarchitectonic boundaries. A consistent characteristic of the dendritic field of all I.O. cells studied was that no dendrite left the confines of the I.O.C., a finding consistent with the observations in other mammals [35,41]. Those neurons positioned at the edge of a subdivision would, of course, be especially affected by this restriction. Thus, a dendrite would turn back into the I.O.C. upon encountering the boundary between the I.O.C. and surrounding tissue such that this restriction on the dendritic domain of a cell resulted in neurons with peculiar dendritic arbors. Neurons on the edge of a subdivision were often seen with dendrites on only one side of the cell or with dendrites still surrounding the soma but forming an asymmetrical field, or, especially with type I neurons, with the distal dendritic branches turned back at the nuclear boundary. We have not illustrated these variations of dendritic field in the typical cells illustrated in Fig. 5 for the sake of simple description. Suffice it to say that both the type I and type II neurons described above can still be recognized regardless of the position of the cell within the cross-sectional dimensions of the I.O. subdivision in which it resides.

Lack of recurrent collaterals in the I.O.C. For many years the issue of the existence of recurrent collaterals from I.O. axons has been addressed (e.g., [35,41]). In fortuitous Golgi-impregnations of adult I.O.C.s, some axons stained and their passage from the nucleus could be observed. Following the course of these axons away from the cell body, the axis cylinder appeared not to branch either within the I.O. subdivision or in its course away from the nucleus. Most axons were observed to cross the midline just dorsal to the I.O.C. before assuming their rostral course toward the cerebellum. These observations from the Golgi material confirmed the impression gained from the Lucifer yellow-filled cells. Indeed Fig. 7B in a previous paper [4] illustrates one such Lucifer yellow-labeled neuron and its axon, and the axon courses away from the I.O.C. without branching. Thus, recurrent collaterals of the axis cylinders of I.O. neurons appeared not to be a prominent feature in the guinea pig.

Types of afferent axons in the I.O.C. From Golgi-impregnations of prenatal guinea pig brainstems, we were able to discern the existence of three afferent axon types as illustrated in Fig. 6, top. The largest axon was relatively smooth with conspicuous varicosities at what appeared to be regular intervals. The other two axons were of smaller calibre and exhibited two different terminal ramifications. One type gave off fine branches at regular intervals, each branch ending in a small chaliced profile. The other small axon type did not give off branches in its trajectory across the subdivision until it ended in a terminal bush-like arrangement. While our survey of afferent axons in the I.O.C. was not exhaustive, it was apparent that all three axon types encountered were present in each subdivision. An examination of the trajectory of the afferent axons indicated that they

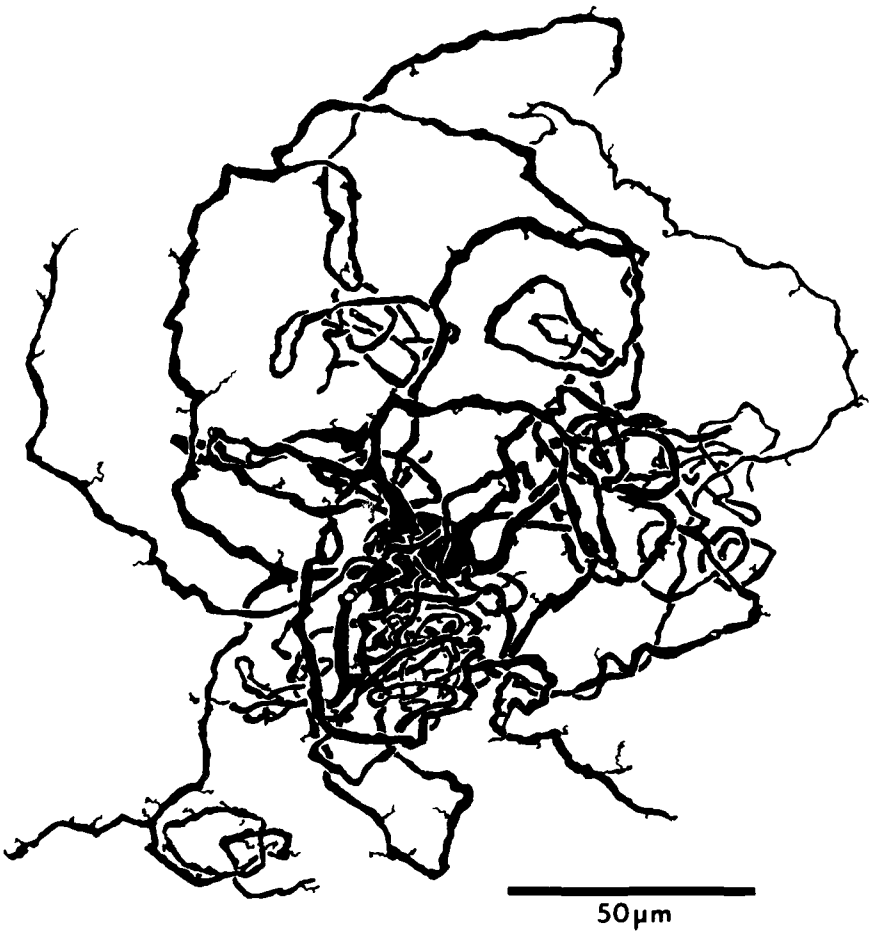
50μm

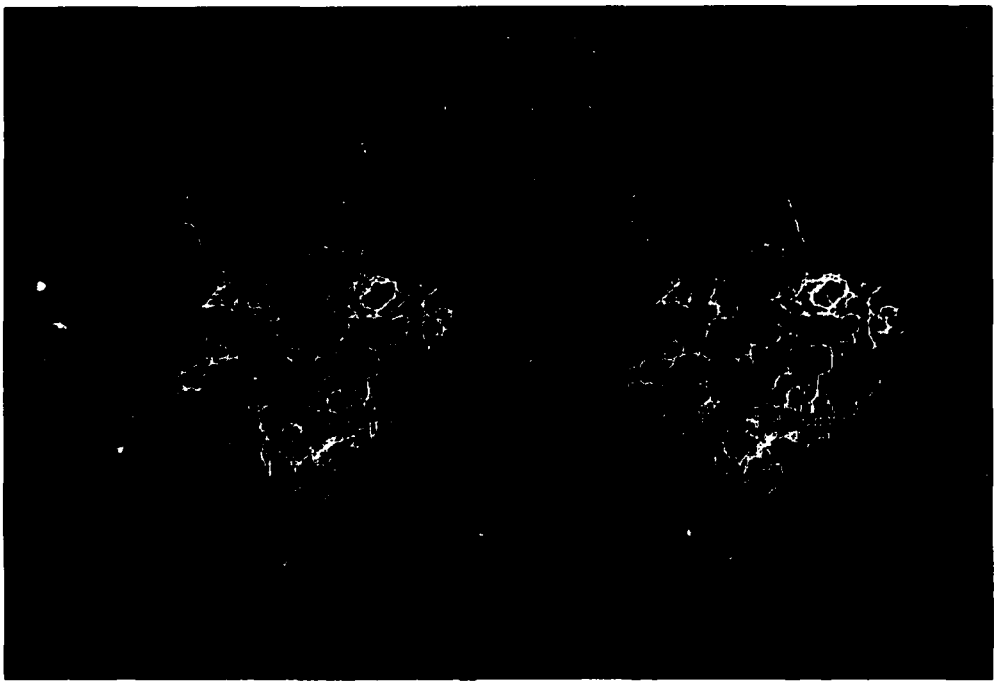

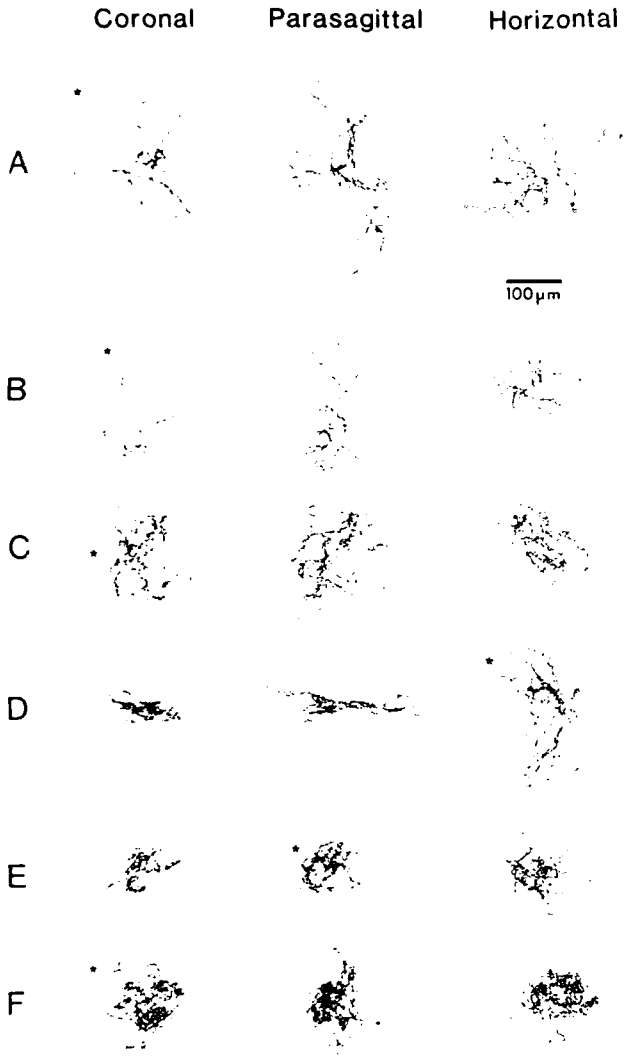

FIG. 5. Stick figure representation of the dendritic arbors of six I.O. cells representing the three dendroarchitectonic cell types. Type I cells are illustrated by A and B, type IIa cells by E and F, and type IIb cells by C and D. The digitized three-dimensional attributes of each cell were used to reconstruct the dendritic tree in the three cardinal section planes. The original section plane of each cell is indicated (*). All cells except D were Golgi-impregnated. Cell D was an HRP labelled cell.

enter the I.O.C. from all directions. Any further analysis of afferent axonal type with regard to any preferred trajectory was not possible with the material at hand.

Relationship of the I.O.C. to adjacent cells in the reticular formation. The apparent restriction of I.O. dendritic fields within the cytoarchitectonic boundaries of the I.O.C., resulting in a so-called 'closed nucleus' [28], leads to the question of whether the neurons of surrounding cell groups might also obey the boundaries of the I.O.C. Not infrequently, the dendrites of isodendritic cells in the reticular formation dorsal to the I.O.C. and dendrites of the large isodendritic cells ventral to the I.O.C. were seen to penetrate an I.O. subdivision and, in some cases, to course completely across the subdivision. Figure 6, bottom illustrates this phenomenon with a camera lucida drawing of two neurons from the scattered marginal isodendritic cells of the ventral I.O.C. It was apparent that these cells, in this case positioned in the hilus between the PO and DAO, send their dendrites into the fringes of an I.O. subdivision. A question arises as to whether the large cells bordering the I.O.C. are displaced type I I.O. cells or type I cells are a subtype of the bordering cells. Based on their soma sizes and dendrite arbors, the cells illustrated in Fig. 6, bottom and the type I I.O. cell illustrated in Fig. 2 (cell B) are dissimilar in that the cells of Fig. 6, bottom are isodendritic cells, whereas those of Fig. 2 are idiodendritic. Isodendritic neurons were never encountered within the confines of the subdivisions of the I.O.C.

DISCUSSION

Cytoarchitecture

The cytoarchitectonic characteristics of the inferior olivary complex appear to be highly conserved across placental mammals. In both its medial-lateral and anterior-posterior aspects, parcellation of the guinea pig inferior olive into medial accessory, dorsal accessory and principal subdivisions concurred with the recent descriptions of the inferior olive in other rodents [6,17], including the further partition of the medial accessory olive into five topological areas. Whether our cytoarchitectonic subdivisions of the guinea pig inferior olive has identified regions homologous to those in other mammals [6–8, 17] awaits the study of the connectional attributes of the subdivisions.

Unlike the inferior olive proper of other mammals [41], large neurons were seldom encountered within the olivary subdivisions of the guinea pig in either Nissl-stained or Golgi-stained sections. Instead, similar large isodendritic neurons either collect into a discrete area located ventrolateral to the nucleus about midway in its anterior-posterior extent or appear scattered at the ventral margins of the subdivisions and into the hilar regions. In lieu of a less nescient designation, we have named the discrete collection of this neuronal type the 'periolivary reticular nucleus' (R; Fig. 1). Whether this nucleus represents a special agglomeration of cells similar to the type scattered along the margins of the nucleus in guinea pig and opossum [7] is unknown, as is their relationship to the large isodendritic cells in the I.O. of other mammals. In fact, the periolivary reticular nucleus in guinea pig may simply be a ventromedial extension of the magnocellular lateral reticular nucleus. A study of the connectional relationship between the periolivary reticular nucleus and the cerebellum or other structures should indicate whether the cell group can be considered as part of the lateral reticular nucleus, the inferior olive or as a unique structure.

FACING PAGE

FIG. 4. Camera lucida drawing (top) and stick figure stereopair (bottom) of a type IIa inferior olive neuron. This Golgi-impregnated cell from a 200 μm thick coronal section displays multiple spiraling dendrites with each dendritic spiral about the size of a cell body. The stereopair illustrates the complexity of this cell in the third dimension and indicates how so much dendrite can be packaged into a small volume. This cell is reconstructed in three section planes in Fig. 5F.

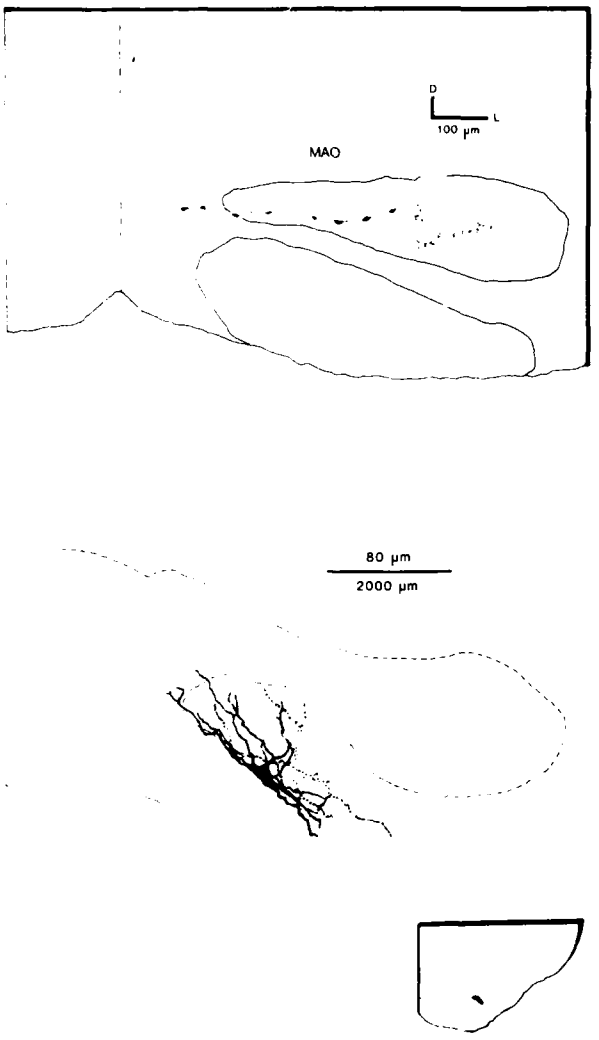

FIG. 6. The I.O. neuropil contains afferent axons and dendrites of surrounding isodendritic cells. TOP—Camera lucida drawing of rapid Golgi impregnated afferent axons in the MAO. The axons illustrated were from three separate sections containing the MAO and are drawn in their respective location and orientation in the composite. Three axonal types are apparent and are typical of those encountered in each I.O. subdivision. BOTTOM—Camera lucida drawing of two isodendritic cells positioned in the hilus between the PO and DAO. These cells have much larger somata compared to I.O. cells and often their olivopetal dendrites penetrate an I.O. subdivision. Dendrites of the large neurons in the reticular formation dorsal to the I.O. (not shown) also penetrate the I.O. neuropil. (Scale bar—lower value is for the inset at lower right.)

Dendroarchitecture

From the earliest descriptions of Golgi-impregnations of the mammalian inferior olivary complex [13, 22, 35, 50], the cells of this nucleus were recognized as some of the more unique in the central nervous system. According to the initial dendroarchitectonic classification scheme of Ramón-Moliner [36], I.O. cells have the characteristics of 'radiate' cells spanning the range of simple 'radiate' to 'radiate-wavy' through a transitional 'intermediate radiate-wavy' form, corresponding to our type I, IIa and IIb cells respectively. In a later classification scheme, Ramón-Moliner [37] placed I.O. cells in the idiodendritic (i.e., peculiar) category which alleviated the confusion arising from the 'radiate' classification of *both* I.O. and reticular formation neurons. Thus, in the guinea pig the large cells of the periolivary reticular nucleus and those cells at the margins of a subdivision would be classified as 'radiate' but could be distinguished from the smaller I.O. neurons by their 'isodendritic' pattern [37,38]. All of the neurons encountered within the guinea pig I.O.C. belong in the idiodendritic category.

An examination of the existing literature has led us to the conclusion that inferior olive cell types, based on dendroarchitectonics, appear to be conserved (typologic conservatism) across placental mammals. Thus, I.O. cells from mouse [35,41], rabbit [35], rat [41], cat [35, 37, 41], dog [41], monkey [41], and human material [13, 22, 35, 41, 50] demonstrate the two basic types of cells. However, the existence across all mammals of a transitional form between the two extreme types cannot be deduced from the literature. Also, whether all cell types across species have approximately eight dendrites and varying degrees of spines and protrusions both on the dendrites and the soma, as do the I.O. cells in guinea pig, is not known. Thus, our supposition that there is typologic conservatism is subjectively based on the drawings and photomicrographs of I.O. cells presented in the literature.

The foregoing interpretation of this study's data in comparison to the extant data is not altogether congruent with the Scheibels' exposition [41]. They have suggested that I.O. dendroarchitectonics change systematically in an evolutionary trend. Their conclusion was based on comparisons between man, monkey and cat material with regard to the diameter of dendritic arbors and concomitant cellular packing densities. The primary idea was that a more compact dendritic tree (e.g., man; Fig. 12 in [41]) was correlated with a lower packing density of cells and that this arrangement was more evolutionarily advanced than a more diffuse dendritic tree and higher packing densities. Their measurement of the diameter of dendritic arbors was necessarily in two-dimensional space and, when cubed, yields V.D.E. measures of 0.008, 0.003, and 0.001 mm^3 for cat, monkey and man respectively. Comparing these data with that derived from the calculated dimensions of a cell's 'principal planes' (V.D.E., Table 2) accurately measured in three-dimensional space, the range of the V.D.E. values from cat-monkey-man almost spans the range of V.D.E. measures in guinea pig. Indeed, if we had taken the smallest dendritic diameter measure in two dimensional space from our data (i.e., smallest of three 'principal planes'; range 100–500 μm) and the smallest dendritic diameters reported by the Scheibels (approximately 100 μm, [41]), there would be complete overlap between man, monkey, cat and guinea pig. Further evidence of the overlap in V.D.E. values across mammals was provided by the analysis of a single primate I.O. neuron (Fig. 3F in [57]) which yielded a V.D.E. value of 0.0037 mm^3 (compare to values in Table 3; also note that the values of I.A. and I.F. for the primate I.O. cell were within the range of those presented in Table 2 herein). Thus, we cannot support the idea of an evolutionary trend in the direction of more compact dendritic trees, and only with a reexamination of data from several diverse species with measurements made in three-dimensions could an accurate estimate of the diversity in dendritic tree volume be made.

Finally, not only does there appear to be cyto- and dendroarchitectonic conservation within the I.O.C. across

species, but the distribution of the cell types within the three primary subdivisions of the inferior olive appears similar between species. The Scheibels [42] noted that, in cat and human, cells similar to those which we call the type I cell were in greatest abundance in the MAO, whereas neurons similar to our type II cells populated the PO and DAO. A similar distribution of cell types across the guinea pig interior olivary complex was noted in our material (Table 1).

Neuronal Classification by Statistics

Classically, neuronal typology based on dendritic arborization has been largely subjective, relying on experience and perceptions of cellular geometry. The early attempts to Sholl [44] and others to provide quantitative descriptors of cell type have been supplemented recently by analytical measures derived from very accurate quantitation of a cell's three-dimensional attributes, a result of advances in computer-assisted microscopy. We have employed quantitative measurements of inferior olive cells and have found that several measures were quite helpful in substantiating our previously subjective neuronal classification.

Procedures from two laboratory groups were adopted for the present study. The first were those of Yelnick, Percheron and colleagues [55–58], who used three generic measures of dendritic form (topologic, geometric, and metric) together with a statistical analysis of the shape and size of the dendritic arbor (principal component analysis). The other procedure was that of Glaser and colleagues [16], who have examined the dendritic trees of cortical neurons in terms of polar and trumpet histograms (analyses which proved to be of little assistance for cells in a nuclear configuration). While the principal component analysis and several topologic, geometric, and metrical parameters provided no criteria for distinguishing I.O. cell types, one topological parameter (branching index, B.I.), one geometrical parameter (index of tortuosity, I.T.), and a metrical parameter (the measure of dendritic arbor volume-V.D.E.) were very useful in statistically defining cell types. Thus, while several metric and geometric descriptors only demonstrated similarities among inferior olive cells, other measures of form supported our subjective, differential typology of the cells.

For statistical descriptions of dendroarchitecture to be generally useful in neuroanatomical studies, the statistics should provide numeric descriptors that can be used for comparisons across studies and for comparisons between cells from other brain regions or other species. In this regard, an examination of the few studies which provide quantitative parameters for the dendritic arbors of several cells lends support to the validity of statistical dendroarchitectonic studies. Thus, the analysis of the dendritic arbor of an inferior olive cell from a primate [57] illustrates the similarity of inferior olive cells across species. Additionally, from the extant quantitative descriptions of central nervous system neurons in mammals, a surprising observation arises. That is, the longest dendrite and total dendritic lengths are similar for various 'radiate' neurons from a variety of brain regions. For example, the total dendritic lengths of an inferior olive cell (this study), a cerebral cortical stellate cell [30], a subthalamic neuron [18,55] and cerebellar Purkinje cells [8,25] are approximately similar. In contrast, large 'radiate' neurons, such as pallidal neurons [56] and spinal cord neurons [10,43], have much greater total dendritic lengths. The apparent difference among cells with similar dendritic length statistics is the geometry of the dendritic arbor. This observation has implications for our understanding of neuronal development. It could be that there is a very restricted gene expression for dendritic length such that there exist only several distinct types of neuron (e.g., neurons with small dendritic arbors, neurons with large dendritic arbors, etc.)

Form Determination in Inferior Olive Cells

From the metrical parameters for the dendritic arbors of type I and type II cells, our results indicate that there is little difference in total dendritic length, area or volume across cell types. This suggests that all inferior olive cells are programmed to produce similar amounts of dendritic and somatic membrane. If so, what factors contribute to the varied dendroarchitectonics of inferior olive neurons? While we can only speculate on the final determinants of form, clearly several variables have to be considered, including developmental factors and the influences of intercellular relationships (i.e., cell-to-cell; afferent axons; efferent organization).

Developmentally, in species examined to date, neurons of the three subdivisions differentiate at various times and migrate to their final positions in two streams of cells [2, 12, 29, 39]. With differential birth dates and migration patterns, the developmental factors could be as simple as cells being derived from separate precursor cells or, if derived from the same precursor cells, as complex as interactions between the timing of cell migration and exogenous factors. The exogenous factors could include afferent innervation, efferent targets, nuclear boundaries and cell-cell relations (i.e., aggregate assemblies of neurons coupled through gap junctions and synaptic glomeruli).

The boundaries of the nucleus are obeyed by the dendrites of I.O. neurons resulting in a 'closed nucleus' [28]. The confines of the nucleus result in some cells displaying dendritic fields on only one side of the cell, and other peculiar geometries. The peculiar geometries are most evident in the type II cells, but type I cells also display alteration of dendritic trajectory at the nuclear boundaries. Since the dendrites of surrounding 'reticular' cells cross the boundaries of the inferior olivary complex, whereas those of inferior olive cells do not, the factors constraining dendritic spread must be asymmetrical operating on inferior olivary but not extrinsic neurons. The nature of such *boundary-factors* is unknown but must constitute an important determinant in final form.

A role for intercellular determinants of form is suggested by the existence of neuronal aggregate organization in the inferior olivary complex. Inferior olive cellular aggregates were demonstrated by Lucifer-yellow dye-coupling [4] and supported by the existence of gap junction contacts between cells [4, 17, 19, 40, 46]. In this regard, membrane differentiations, such as gap junctions, may require precise cell-to-cell relations. Hence, the number of gap junctions per dendrite and their position might influence form. For example, if a type I cell requires only a few gap junctions whereas a type II requires multiple contacts, dendritic geometry could be determined by the dendritic trajectories necessary to establish few or multiple contacts. Finally, the synaptic glomeruli of the inferior olive [20] represent another type of intercellular relation requiring precise dendritic localization. If nuclear boundaries and intercellular relations are form determinants, an examination of inferior olive cells during development and/or in dissociated cell cultures might provide useful insights into the relative contribution of these two factors.

A final exogenous factor which could influence dendritic form is the afferent and efferent organization of the nucleus. We have described three axon types with distribution patterns into all three subdivisions; two of the types are similar to early descriptions [35,42] of inferior olive afferents. Whether any one of these influence dendritic arbor formation is unknown. However, based on the apparent heterogeneous distribution of axon types across the inferior olivary complex, it has been argued [42] that afferents have a minimum role in form determination. There remains, however, the distinct possibility that one afferent axon type makes contact with only one inferior olive cell type, thereby providing a substrate for form determination. In the absence of a detailed, three-dimensional reconstruction of axodendritic relations for the inferior olive cell types, afferent axonal arbors must remain only a possible factor in the definition of dendritic geometry.

Neuroanatomical Correlates of Inferior Olive Neurophysiology

Oscillatory behavior of inferior olive neurons appeared to be a cellular feature common to all neuronal types in the complex. From the data presented in a preceding paper [4], cells of both type I and type II varieties were observed to display calcium-dependent oscillations of their membrane potential. Lucifer yellow dye-coupling between cells of both types was also observed, together with the anatomical substrate for dye-coupling and electrotonic neurotransmission, the gap junction. Other data demonstrated that, in some instances, more than one cell was labelled by dye-coupling, suggesting that an aggregate assembly of several inferior olive neurons might form a functional unit. The anatomical data from the present study together with previously published observations on the cat I.O.C. (Figs. 14 and 15 in [41]) are entirely consistent with the idea that the inferior olivary complex is organized into cellular aggregates which can behave much like an electrical syncytium. An aggregate assembly of type I cells might be predicted to be less compact or contain fewer cells than one composed of type IIa cells, possibly a simple reflection of the breadth of the dendritic field of each cell type. Circumstantial support for this prediction comes from the observation that Lucifer yellow dye-coupling [4] of type I cells rarely involved more than two or three cells while dye coupling between type II cells often illustrated a five or six neuron aggregate. The anatomical and neurophysiological relationship of the aggregate organization to the afferent and efferent connectional characteristics of each I.O. subdivision is open to study. Whether all inferior olive neurons participate in cellular aggregates is unknown.

Of considerable importance to the understanding of inferior olive integrative neurophysiology was the previous finding [4] that presumed stimulation of afferent axons damped or completely shut-off an inferior olive cell's oscillatory behavior. The present study described three axonal types which innervate the inferior olivary complex and similar afferent types have also been seen in the I.O.C. of other mammals [35,41]. At issue is the anatomical substrate of the physiological damping. The large beaded axon and the axon with multiple chaliciform terminal arbors were reminiscent of monoaminergic axons described in a multitude of histochemical and immunocytochemical studies (e.g., [5, 11, 21, 45, 48, 52–54]). Based on the recent electrophysiological evidence of Llinás and Yarom [27] and the results of experiments utilizing a monomaine oxidase inhibitor [26,31], axon types that are serotonin- or dopamine-containing would be excitatory and those containing noradrenalin would be the source of inhibition or damping. Whether excitatory and inhibitory monoamines partition into these two anatomically distinct axon types is unknown. The source and neurochemical identity of the third type of axon telodendria in the I.O., the bush-type arbor, are also unknown. Since a wide range of brainstem and spinal cord structures project to the inferior olivary complex (e.g., [11]), the bush-type arbors may arise from a host of sources. Indeed, it is apparent that non-monoaminergic sources, such as spinal cord afferents, are excitatory to the I.O. [3]. The careful definition of sources of afferent axonal types as a function of whether they either excite inferior olive cells into spiking rhythmically or inhibit endogenous rhythmic activity is crucial to the understanding of inferior olive information processing.

ACKNOWLEDGEMENTS

We thank Dr. L. Eisenman for helpful discussion on inferior olive cytoarchitecture and Dr. N. McMullen for discussions on tortuosity descriptors. The computer software used for quantitative analyses was developed by the DAKKRO Corp., Denver, CO. We thank Dr. R. Sweeney and his staff for their programming efforts. We acknowledge the technical assistance of K. Olson, T. Kerns and C. Cullum. This work was supported by the U.S. Army Medical Research and Development Command.

REFERENCES

1. Adams, J. C. A fast, reliable silver chromate Golgi method for perfusion-fixed tissue. *Stain Technol* **54:** 225–226, 1979.
2. Altman, J. and S. A. Bayer. Prenatal development of the cerebellar system in the rat. II. Cytogenesis and histogenesis of the inferior olive, pontine gray, and the precerebellar reticular nuclei. *J Comp Neurol* **179:** 49–76, 1978.
3. Armstrong, D. M. Functional significance of connections of the inferior olive. *Physiol Rev* **54:** 358–417, 1974.
4. Benardo, L. S. and R. E. Foster. Oscillatory behavior in inferior olive neurons: Mechanisms, modulation, cell aggregates. *Brain Res Bull* **17:** 773–784, 1986.
5. Bishop, G. A. and R. H. Ho. Substance P and serotonin immunoreactivity in the rat inferior olive. *Brain Res Bull* **12:** 105–113, 1984.
6. Blatt, G. J. and L. M. Eisenman. A qualitative and quantitative light microscopic study of the inferior olivary complex of normal, reeler, and weaver mutant mice. *J Comp Neurol* **232:** 117–128, 1985.
7. Bowman, M. H. and J. S. King. The conformation, cytology and synaptology of the opossum inferior olivary nucleus. *J Comp Neurol* **148:** 491–524, 1973.
8. Brodal, A. and K. Kawamura. Olivocerebellar projection: A review. *Adv Anat Embryol Cell Biol* **64:** 1–137, 1980.
9. Calvet, M.-C., J. Calvet, R. Camacho and D. Eude. The dendritic trees of Purkinje cells: a computer assisted analysis of HRP labeled neurons in organotypic cultures of kitten cerebellum. *Brain Res* **280:** 199–215, 1983.
10. Cameron, W. E., D. B. Averill and A. J. Berger. Quantitative analysis of the dendrites of cat phrenic motoneurons stained intracellularly with horseradish peroxidase. *J Comp Neurol* **230:** 91–101, 1985.
11. Courville, J., Y. Lamarre and C. Mentigny (Eds.) *The Inferior Olivary Nucleus: Anatomy and Physiology*. New York: Raven Press, 1980.

12. Ellenberger, C., J. Hanaway and M. G. Netsky. Embryogenesis of the inferior olivary nucleus in the rat: A radioautoradiographic study and re-evaluation of the rhombic lip. *J Comp Neurol* **137:** 71–88, 1969.
13. van Gehuchten, A. *Anatomie du Systeme Nerveux de l'Homme*. Louvian, Librairie Universitaire, A. Uystpruyst-Dieudonne, 1905, pp. 510–524.
14. Geisert, E. E., Jr. and B. V. Updyke. Chemical stabilization of Golgi silver chromate impregnations. *Stain Technol* **52:** 137–141, 1977.
15. Glaser, E. M. A binary identification system for use in tracing and analyzing dichotomously branching dendrite and axon systems. *Comput Biol Med* **11:** 17–19, 1981.
16. Glaser, E. M., H. Van der Loos and M. Gissler. Tangential orientation and spatial order in dendrites of cat auditory cortex: A computer microscope study of Golgi-impregnated material. *Exp Brain Res* **36:** 411–431, 1979.
17. Gwyn, D. G., G. P. Nicholson and B. A. Flumerfelt. The inferior olivary nucleus of the rat: A light and electron microscopic study. *J Comp Neurol* **174:** 489–520, 1977.
18. Hammond, C. and J. Yelnik. Intracellular labeling of rat subthalamic neurones with horseradish peroxidase: computer analysis of dendrites and characterization of axon arborization. *Neuroscience* **8:** 781–790, 1983.
19. King, J. S. The synaptic cluster (glomerulus) in the inferior olivary nucleus. *J Comp Neurol* **165:** 387–400, 1976.
20. King, J. S. Synaptic organization of the inferior olivary complex. In: *The Inferior Olivary Nucleus: Anatomy and Physiology*, edited by J. Courville, Y. Lamarre and C. Mentigny. New York: Raven Press, 1980, pp. 1–33.
21. King, J. S., R. H. Ho and R. W. Burry. The distribution and synaptic organization of serotoninergic elements in the inferior olivary complex of the opossum. *J Comp Neurol* **227:** 357–368, 1984.
22. von Kolliker, A. (cited by Cajal). *Handbuch der Gewebelehre des Menschen*, 6th edition, 1893.
23. Llinas, R. Rebound excitation as the physiological basis for tremor: a biophysical study of the oscillatory properties of mammalian central neurones *in vitro*. In: *Movement Disorders: Tremor*, edited by L. J. Findley and R. Capildeo. New York: Macmillan, 1984, pp. 165–182.
24. Llinas, R., R. Baker and C. Sotelo. Electrotonic coupling between neurons in cat inferior olive. *J Neurophysiol* **37:** 560–571, 1974.
25. Llinas, R. and D. E. Hillman. A multipurpose tridimensional reconstruction computer system for neuroanatomy. In: *Golgi Centennial Symposium: Perspectives in Neurobiology*, edited by M. Santini. New York: Raven Press, 1975, pp. 71–91.
26. Llinas, R. and R. A. Volkind. The olivo-cerebellar system: functional properties as revealed by harmaline-induced tremor. *Exp Brain Res* **18:** 69–87, 1973.
27. Llinas, R. and Y. Yarom. Oscillatory properties of guinea-pig inferior olivary neurones and their pharmacological modulation: An *in vitro* study. *J Physiol* **376:** 163–182, 1986.
28. Mannen, H. Noyau ferme et noyau ouvert. *Arch Ital Biol* **98:** 333–350, 1960.
29. Marchand, R. and L. Poirier. Autoradiographic study of the neurogenesis of the inferior olive, red nucleus and cerebellar nuclei of the rat brain. *J Hirnforsch* **23:** 211–224, 1982.
30. McMullen, N. T., E. M. Glaser and M. Tagamets. Morphometry of spine-free nonpyramidal neurons in rabbit auditory cortex. *J Comp Neurol* **222:** 383–395, 1984.
31. Montigny, C. de and Y. LaMarre. Rhythmic activity induced by harmaline in the olivocerebello-bulbar system of the cat. *Brain Res* **53:** 81–95, 1973.
32. Morest, D. K. The Golgi methods. In: *Techniques in Neuroanatomical Research*, edited by Ch. Heym and W.-G. Forssmann. New York: Springer-Verlag, 1981, pp. 124–138.
33. Oscarsson, O. and B. Sjölund. The ventral spino-olivocerebellar system in the cat. III. Functional characteristics of the five paths. *Exp Brain Res* **28:** 505–520, 1977.
34. Rall, W. Core conductor theory and cable properties of neurons. In: *Handbook of Physiology, Volume I. Cellular Biology of Neurons, Part 1, Section 1: The Nervous System*, edited by E. R. Kandel. Bethesda: American Physiological Society (Baltimore: The Williams and Wilkins Co.), 1977, pp. 39–97.
35. Ramón y Cajal, S. *Histologie du Système Nerveux de l'Homme & des Vertèbrés*. Madrid: Instituto Ramón y Cajal, 1952 edition, pp. 912–933.
36. Ramón-Moliner, E. An attempt at classifying nerve cells on the basis of their dendritic patterns. *J Comp Neurol* **119:** 211–227, 1962.
37. Ramón-Moliner, E. The morphology of dendrites. In: *The Structure and Function of Nervous Tissue*, edited by G. H. Bourne. New York: Academic Press, 1968, pp. 205–267.
38. Ramón-Moliner, E. and W. J. H. Nauta. The isodendritic core of the brainstem. *J Comp Neurol* **126:** 311–336, 1966.
39. Robertson, L. T. and W. A. Stotler. The structure and connections of the developing inferior olivary nucleus of the rhesus monkey (*Macaca mulatta*). *J Comp Neurol* **158:** 167–190, 1974.
40. Rutherford, J. G. and D. G. Gwyn. Gap junctions in the inferior olivary nucleus of the squirrel monkey, *Saimiri sciureus*. *Brain Res* **128:** 374–378, 1977.
41. Scheibel, M. E. and A. B. Scheibel. The inferior olive. A Golgi study. *J Comp Neurol* **102:** 77–132, 1955.
42. Scheibel, M., A. Scheibel, F. Walberg and A. Brodal. Areal distribution of axonal and dendritic patterns in inferior olive. *J Comp Neurol* **106:** 21–49, 1956.
43. Sedivec, M. J., J. J. Capowski and L. M. Mendell. Morphology of HRP-injected spinocervical tract neurons: Effect of dorsal rhizotomy. *J Neurosci* **6:** 661–672, 1986.
44. Sholl, D. A. *The Organization of the Cerebral Cortex*. London: Methuen, 1956.
45. Sjölund, B., A. Björklund and L. Wiklund. The indolaminergic innervation of the inferior olive. 2. Relation to harmaline induced tremor. *Brain Res* **131:** 23–37, 1977.
46. Sotelo, C., R. Llinás and R. Baker. Structural study of inferior olivary nucleus of the cat: morphological correlates of electrotonic coupling. *J Neurophysiol* **37:** 541–559, 1974.
47. Stewart, W. W. Functional connections between cells as revealed by dye-coupling with highly fluorescent naphthalimide tracer. *Cell* **14:** 741–759, 1978.
48. Takeuchi, Y. and Y. Sano. Immunohistochemical demonstration of serotonin-containing nerve fibers in the inferior olivary complex of the rat, cat and monkey. *Cell Tissue Res* **231:** 17–28, 1983.
49. Uylings, H. B. M., G. J. Smith and W. A. M. Veltman. Ordering methods in quantitative analysis of branching structures of dendritic trees. *Adv Neurol* **12:** 247–254, 1975.
50. Vincenzi, L. *Sulla fina Anatomia dell 'uomo*. Estr. della Real. Accad. Medic. di Roma II, 3 (cited in Ramón y Cajal), 1886–1887.
51. Wann, D. F., T. A. Woolsey, M. L. Dierker and W. M. Cowan. An on-line digital-computer system for the semiautomatic analysis of Golgi-impregnated neurons. *IEEE Trans Biomet Eng* **20:** 233–247, 1973.
52. Wiklund, L., A. Björklund and B. Sjölund. The indolaminergic innervation of the inferior olive. I. Convergence with the direct spinal afferents in the areas projecting to the cerebellar anterior lobe. *Brain Res* **131:** 1–21, 1977.
53. Wiklund, L., L. Descarries and K. Møllgård. Serotoninergic axon terminals in the rat dorsal accessory olive: normal ultrastructure and light microscopic demonstration of regeneration after 5,6-dihydroxytryptamine lesioning. *J Neurocytol* **10:** 1009–1027, 1981.
54. Wiklund, L., B. Sjölund and A. Björklund. A morphological and functional study on the serotoninergic innervation of the inferior olive. *J Physiol (Paris)* **77:** 183–186, 1981.
55. Yelnik, J. and G. Percheron. Subthalamic neurons in primates: a quantitative and comparative analysis. *Neuroscience* **4:** 1717–1743, 1979.

56. Yelnik, J., G. Percheron and C. François. A Golgi analysis of the primate globus pallidus. II. Quantitative morphology and spatial orientation of dendritic arborizations. *J Comp Neurol* **227:** 200–213, 1984.

57. Yelnik, J., G. Percheron, C. François and Y. Burnod. Principal component analysis: a suitable method for the 3-dimensional study of the shape, dimensions and orientation of dendritic arborizations. *J Neurosci Methods* **9:** 115–125, 1983.

58. Yelnik, J., G. Percheron, J. Perbos and C. François. A computer-aided method for the quantitative analysis of dendritic arborizations reconstructed from serial sections. *J Neurosci Methods* **4:** 347–364, 1981.